A novel procedure for accurately measuring the Mode II fracture toughness of steel fiber reinforced self-compacting concrete

Mennat-Allah Hossam El-Din, Mohamed Moawad, Seleem S. E. Ahmad
Faculty of Engineering, Zagazig University, Egypt
m.salam22@eng.zu.edu.eg, https://orcid.org/0009-0006-1270-7216
mamoawad@zu.edu.eg, http://orcid.org/0000-0002-6806-900X
ssdawod@eng.zu.edu.eg, http://orcid.org/0000-0001-9894-0209

Ramy M. Reda
Higher Technological Institute, Egypt
ramy.mostafa@hti.edu.eg, http://orcid.org/0000-0002-3298-7925

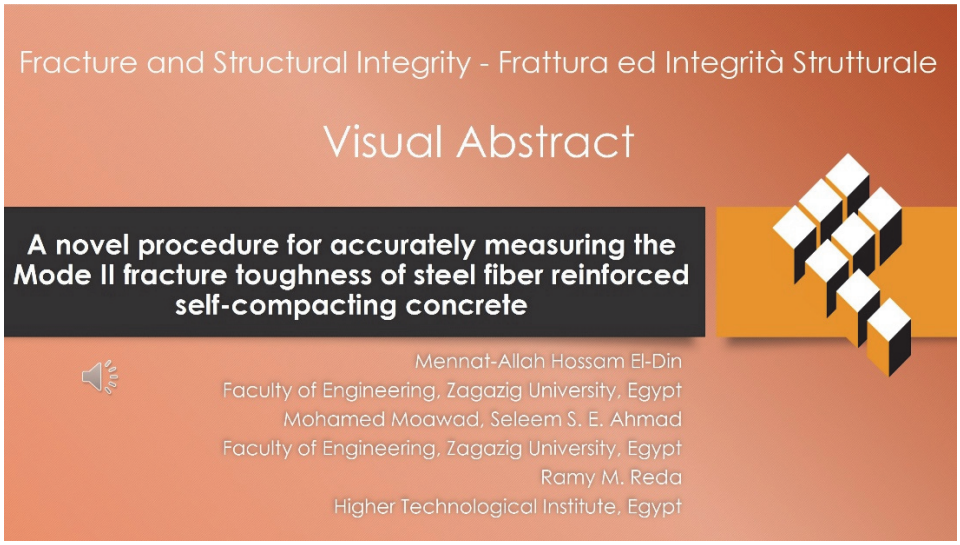

KEYWORDS: Steel fiber reinforced self-compacting concrete, Mode II fracture toughness, Through-thickness crack, Matrix crack, Fiber bridging effect.

OPEN ACCESS

Citation: Hossam El-Din, M. A., Moawad, M, Ahmad, S.S.E., Reda, R. M.A novel procedure for accurately measuring the Mode II fracture toughness of steel fiber reinforced self-compacting concrete, Fracture and Structural Integrity, 75 (2026) 200-212.

Received: 31.08.2025
Accepted: 28.10.2025
Published: 31.10.2025
Issue: 01.2026

INTRODUCTION

Self-compacting concrete (SCC), a category of high-performance concrete, is a specialized material first developed by Japanese researchers. It provides enough cohesion to prevent segregation or bleeding. This advanced concrete is designed to fill formwork spaces under its own weight without mechanical vibration, a solution driven by the demand for casting narrow, highly reinforced structures. Using SCC accelerates the construction process and reduces

labor costs while avoiding issues like porous concrete and weak bonding that can occur with traditional concrete in congested zones. While SCC retains the brittleness and crack propagation behavior typical of conventional concrete, embedding fibers within the matrix/concrete, named fiber reinforced concrete (FRC), has proven effective in enhancing the tensile and flexural performance, increasing toughness, and superior energy absorption of fiber reinforced self-compacting concrete (FRSCC) [1-2]. Adding the fibers to concrete involves various variables, including their shape, length, and cross-section. Hooked-end steel fibers significantly contribute to enhancing concrete performance. Although the inclusion of steel fibers enhances the mechanical performance of SCC, it also leads to noticeable challenges in the fresh state of SCC. As a result, these changes can negatively influence the mix's flowability, passing ability, and segregation resistance. Several studies have shown that low fiber volume fraction percentage (Vf%) can still enhance performance, especially when workability is a key concern [1].

On the other hand, fracture has emerged as a key concern in structural analysis and design [3-6]. Despite the extensive research on the mode I (tension mode) fracture toughness of FRC [3,5], investigations into pure mode II (sliding mode) fracture toughness remain relatively limited. However, mode II plays a vital role in structural situations involving jointed interfaces, interfacial cracks, or shear-induced slip in concrete components, where sliding governs crack behavior [1,6]. The most common specimen geometries used to obtain mode II were: double notched cube (DNC) [7-9], double-edge notched prism (DENP) [10], short core in compression [11], and Punch-through shear (PTS) [12]. Previous investigations into the fracture toughness of fibrous composite materials were limited by their reliance on through-thickness cracked (TTC) specimens, whether in concrete, FRC, composites, or rock. It is worth noting that TTC may apply to monolithic materials, such as pre-cracked plain concrete without fibers. However, fibers play a critical role in mode II fracture toughness (K_{IIC}) in fibrous composites by resisting shear sliding through bridging cross-matrix cracks. This bridging mechanism is entirely absent in TTC, which leads to the neglect of fiber contribution, an engineering drawback that limits the realistic assessment of fracture behavior. Cai et al. [8] concluded that the use of fibers effectively increases the resistance of concrete to shear cracking and unstable fracture. The K_{IIC} did not change significantly with increasing a/w, which was similar to the results of Watkins [7]. However, some studies found that the shear fracture toughness decreased with increasing a/w for DNC specimens, which may be attributed to the fact that the shorter fracture path accelerates specimen damage at low loads. The reason for the different K_{IIC} trends may be related to the specimen size [8].

To overcome this dilemma, Sallam and co-workers [13-19] proposed an innovative method by introducing the use of matrix cracks (MC) to preserve fiber bridging in the case of pure mode I and mixed mode I and II cracks, representing a significant step toward achieving more realistic fracture behavior. Ali et al. [13] studied the effect of increasing the notch depth to beam depth (a/w) on mode I fracture toughness (K_{IC}) values. Three different a/w ratios were investigated: 0.1, 0.3, and 0.5, and the difference between MCs and TTCs in analyzing K_{IC}. The results showed that, as the a/w ratio increased, the mode I fracture toughness K_{IC} decreased. Specifically, increasing a/w from 0.1 to 0.3 resulted in decreases in crack initiation and peak loads by 21.9% and 21%, respectively. When rising from 0.1 to 0.5, these values decreased by 39.1% and 25.1%, respectively. On the other hand, the research indicated that the TTC specimens showed identical crack initiation and peak loads, reflecting the absence of fiber bridging in those specimens. In contrast, MC specimens exhibited a significant drop in the descending part of the load-deflection curve with an increase in the a/w ratio [13]. Abdallah et al. [17] focused on several key variables related to the K_{IC} of fibrous concrete. The research studied two different fiber volume fractions, specifically 1% and 2%, and involved different a/w ratios, with values ranging from 0.1 to 0.6, to observe their effects on K_{IC}; the distinction between MCs and TTCs was crucial in analyzing their respective impacts on the K_{IC}. Their results showed that increasing the fiber content was found to enhance the K_{IC}, indicating a positive correlation between fiber content and the values of K_{IC}. In contrast, increasing the a/w ratio from 0.1 to 0.3 resulted in a decrease in peak loads by 36.7%, while from 0.3 to 0.5, it reduced peak loads by 9.5%. The higher a/w ratios led to increased toughness. On the other hand, the MC beam specimen yields a realistic mode I fracture toughness value by incorporating the effect of fiber bridging across the pre-crack [13-18].

The effect of the ratio between span length to depth (L/d) and the size of the beams on mode I fracture toughness K_{IC} was investigated by Elakhras et al. [14-16]. The L/d was taken as 4, 5, and 6. Also, the influence of fiber bridging on crack closure and overall fracture resistance was focused on. It can be concluded that, in matrix-cracked beams, the K_{IC} is primarily determined by the depth of the pre-crack. For a given pre-crack depth, the value of K_{IC} remains relatively constant, regardless of the beam's L/d ratio. This dependency on pre-crack depth distinguishes their behavior from beams with through-thickness cracks [14-16]. Hussien et al. [19] studied the effect of mode of mixity, crack offsets, fiber length, beam configuration, and fracture surface patterns of TTC and MC specimens on mixed-mode fracture toughness. From their results, it can be concluded that MC specimens showed different crack initiation behaviors than TTC specimens. Specifically, the crack initiated before the peak load in MC specimens, while it occurred at the peak load in TTC specimens. Additionally, the load drop was gradual in MC specimens but sharp in TTC specimens, highlighting the effect of fiber bridging across the pre-crack [19].

In a recent study published online on September 12, 2025, Cai et al. [8] studied the effect of a/w on the K_{IIC} of FRC using DNC TTC specimens, this means, or in other words, to the best of the authors' knowledge, that no research has been found in the literature to date addressing the K_{IIC} of FRC using MC specimens. Therefore, the main object of this study is to introduce the novel experimental approach by employing DNC specimens with MC to accurately measure K_{IIC}, addressing the limitations of previous studies that relied on TTC and failed to capture the realistic fiber bridging effect. Various a/w, which equal 0.3, 0.4, and 0.5, and Vf% equals 1 and 1.5% were investigated. Three series of fiber arrangement, as well as an SCC without fibers, were considered for comparison to illustrate the effect of the presence of intact fibers (fiber bridge) on the pre-notch surfaces on the accuracy of K_{IIC} measurement for FRSCC: First, TTC specimens, second, MC specimens, and third, the fibers were dispersed between the two pre-notch surfaces (fiber bridging existed) while the specimens were completely cast without fibers (MC/C), i.e., SCC specimens without fibers. A major contribution of the current study is the comparison of the K_{IIC} measured from TTC and MC/C specimens, which shows the efficiency of fibers behind the crack tip in resisting crack growth, and those ahead of the crack tip.

EXPERIMENTAL WORK

Materials and mix proportions

SFRSCC was designed for the experimental program. Type I Portland cement with grade 42.5N was used. Coarse aggregate (dolomite) with NMS 10 mm and specific gravity of 2.7 was used; natural siliceous sand with a specific gravity of 2.55 was used. The physical and mechanical properties of the coarse and fine aggregates are listed in Tab. 1. High water reduced the named Viscocrete-3425 from Sika Company, with 1.5% of the cement weight used to produce SCC, the water-cement (W/C) ratio was 0.4. On the other hand, hooked-end steel fibers of 50 mm in length and 1.0 mm in diameter were used by a Vf% of 1 and 1.5%, the tensile strength and density of the used fibers were 1200 MPa and 7.87 t/m^3, respectively. The hooked-end steel fibers benefit from their strong bond with the cement matrix and better flexural performance. SCC was designed to achieve 30 MPa in compressive strength; the mix proportions of SCC with Vf% = 1% are listed in Tab. 2.

The fresh concrete properties of SCC were measured just after mixing, through the following tests: the slump flow, T50, V-funnel, and L-box tests according to EFNARC [20]. The fresh property results of SCC with Vf% = 1% are listed in Tab. 3. The Table shows that all mixes were within acceptable limits according to EFNARC [20].

Coarse aggregate (dolomite)		Fine aggregate	
Property	Measured Value	Property	Measured Value
Specific gravity	2.7	Specific gravity	2.50
Unit weight, (t/m^3)	1.455	Unit weight, (t/m^3)	1490
Absorption, %	0.86 %	Fine material (75 μ)	1.1 %
Crushing value, %	23.73		
Impact value, %	11.92		
Los Angeles value, %	17.4		

Table 1: Coarse and fine aggregates' physical and mechanical properties.

Cement	Water	Sand	Dolomite	Steel Fiber	Admixture (1.5%)
400	160	970	970	79	6.0

Table 2: SCC mix proportions with Vf% = 1% in kg/m^3.

Property	Slump Flow (mm)	T50 (sec)	V-Funnel time (sec)	L-box (ratio)
Measured value	730	3.0	7.3	0.96
Acceptance criteria (EFRNARC) [20]	600-800	2-5	6-12	0.8-1

Table 3: Fresh Properties of SCC with Vf% = 1%.

The compressive strength of SCC was measured by testing 150 mm side length cubes [21], and indirect tensile strength was measured by testing 300 mm height and 150 mm diameter cylinders [22]. The specimens were demolded 24h after casting and cured for 28 days before testing. The compressive and indirect tensile strengths for SCC without fiber were 31.5 MPa and 3.0 MPa, respectively. Incorporating hooked-end steel fibers into SCC slightly improved its compressive strength by 1.19 and 1.24 for Vf% = 1% and 1.5%, respectively, while the improvement in direct tensile strength equals 1.62 and 1.78 for Vf% = 1% and 1.5%, respectively.

Experimental program

The shear strength of concrete was measured using the push-off specimens, the most common specimen (L-shape specimen) consisting of two L-shaped blocks connected by a tie through which the shear load is applied. The geometry and dimension details of the L-shape specimen are found elsewhere [23]. The shear strength of SCC with and without fibers was measured through L-shape specimens. Double-notched cube (DNC) specimens were selected due to their practical simplicity and proven capability to promote K_{IIC}. The dimensions of the DNC specimens were 150 mm cubes (w = 150 mm), as shown in Fig. 1; three different values of notch depth to specimen width ratio (a/w) equal to 0.3, 0.4, and 0.5, i.e., a = 45, 60, and 75 mm, were used. A total of seventy-five specimens were divided into four series and tested to evaluate K_{IIC}. For the reliability study for DNC specimens, the maximum shear stresses were measured through DNC specimens ($\sigma_{Max\text{-}Shear} = P_{Ultimate}/[(w\text{-}a) \times w]$) and compared with those measured through L-shape specimens, as listed in Tab. 4. It is clear from Tab. 4 that the difference between them ranged between ±8%.

First series; (SCC) specimens without fibers, second series; (MC/C configuration) the fibers were only presented along the pre-notch surfaces with a Vf% equals to 1% leaving the rest of specimen without fibers, third series; (TTC configuration) the fibers were distributed throughout the entire specimen with Vf% equals to 1% and no fibers existed between the pre-notch surfaces. Finally, the fourth series (MC configuration) fibers were uniformly distributed throughout the entire specimen, and the fabricated MC surface had a Vf% % equal to 1 and 1.5%. Five specimens for each case were tested to ensure statistical reliability. The configuration of the four series was shown and described in Fig. 2 and Tab. 5. To the best of the authors' knowledge, the concept of matrix-cracked specimens has not yet been adopted for measuring the real mode II fracture toughness in FRCs; see e.g. [8].

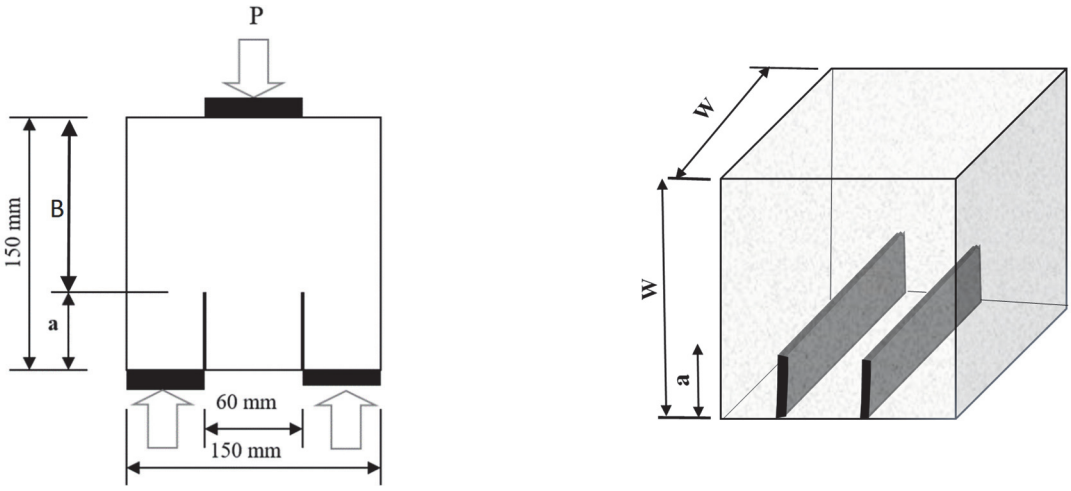

Figure 1: Specimen geometry: w=150 mm, a/w= 0.3, 0.4, and 0.5

Mix	L-shape	Maximum Shear Stress (MPa) DNC with a/w = 0.3	0.4	0.5	Average	Comparison [(L-shape-DNC)/Lshape]%
SCC	5.18	4.4	5.04	5.08	4.84	6.6%
SCC with Vf%=1%	7.04	7.05	7.46	8.18	7.56	-7.4%
SCC with Vf%=1.5%	9.78	8.09	8.51	11.01	9.2	5.9%

Table 4: Comparison between the shear strength measured through L-shape and DNC specimens.

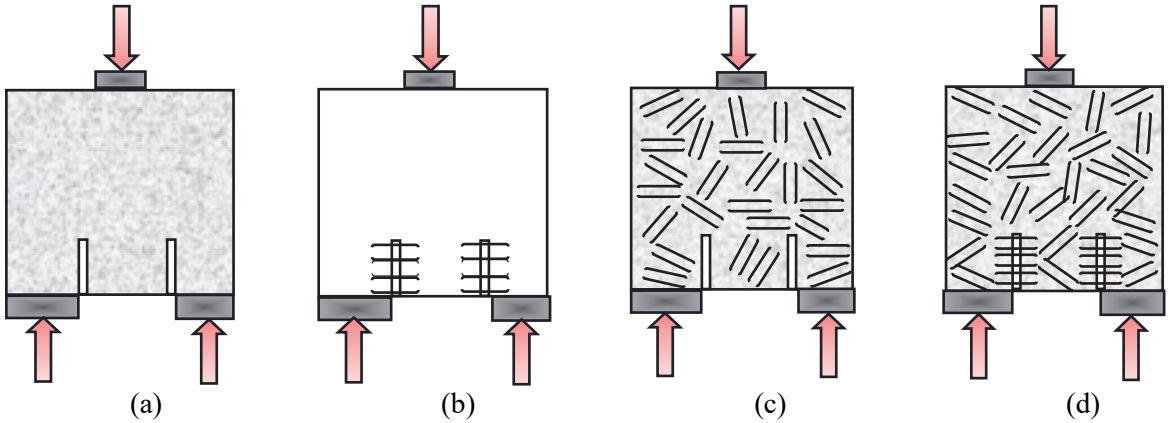

Figure 2: Specimens configuration according to fiber arrangement; (a) SCC, (b) MC/C, (c) TTC, (d) MC.

Matrix crack-preparing and test setup

To simulate realistic Mode II fracture behavior, MC specimens were prepared by inserting two foam panels of 2 mm in thickness in the mold; the foam dimensions matched the intended crack lengths, one-third of the total number of steel fibers representing Vf% of 1 or 1.5% was fixed in the foam panel using adhesive material. After the specimens had cured and before testing, the foam panel was removed by dissolving it with gasoline to demonstrate the fiber bridging effect. MC preparation steps were shown in Fig. 3. This technique was adopted by Sallam and co-workers [13-17, 19]. This setup allowed steel fibers to bridge the pre-notch surfaces, enabling a more realistic representation of fracture behavior in fibrous composites. In the case of the TTC specimens, the crack was cut with a saw to obtain a fiber-free surface and ensure that no bridging fibers remained on the pre-crack surfaces.

Series	Series name	Specimen ID	Fiber arrangement	Vf%	a/w
1st	SCC	SCC-0.3 SCC-0.4 SCC-0.5	-	-	0.3, 0.4, and 0.5
2nd	MC/C	MC/C 1%-0.3 MC/C 1%-0.4 MC/C 1%-0.5	Only at the fabricated MC surface	1.0 %	0.3, 0.4, and 0.5
3rd	TTC	TTC 1%-0.3 TTC 1% -0.4 TTC 1% -0.5	Distributed throughout the entire specimen (no fiber at the crack)	1.0 %	0.3, 0.4, and 0.5
4th	MC	MC 1%-0.3 MC 1%-0.4 MC 1%-0.5 MC 1.5% -0.3 MC 1.5% -0.4 MC 1.5% -0.5	Distributed throughout the entire specimen and the fabricated MC surface	1.0 % 1.5 %	0.3, 0.4, and 0.5

Table 5: Configuration of test specimens.

The specimens were tested using a hydraulic compression testing machine with a maximum load capacity of 2000 kN, conforming to the BS 1881-115 [24]. The machine was used to apply compressive loading vertically on the specimens until failure. To ensure proper load transfer and accurate crack propagation under shear, three steel plates were placed symmetrically at each specimen's base and loading points, aligned with the notches. Fig. 4 shows the test setup. The specimens were loaded under loading control with a rate of 200 Ns^{-1} as suggested by Prokopski [9]. In the present stage of the analysis/work, the ultimate load was utilized only. Although the loading rate condition does not need an expensive testing machine, after the onset of unstable crack growth, it wasn't easy to control the loading process. Image processing was employed to measure the crack mouth sliding displacement (CMSD) through a digital camera (Nikon D5300), as

shown in Fig. 4. The value was measured by calculating the difference between the vertical displacements of the two points on the opposite surfaces of the pre-crack. The first point was placed on the right side near the crack mouth, while the second point was placed on the left side. Some of the tested specimens will be tested under displacement control to complete the CTSD analysis, i.e., to capture CMSD when the unstable crack growth occurred at and after the ultimate load, and this analysis will be presented in future work.

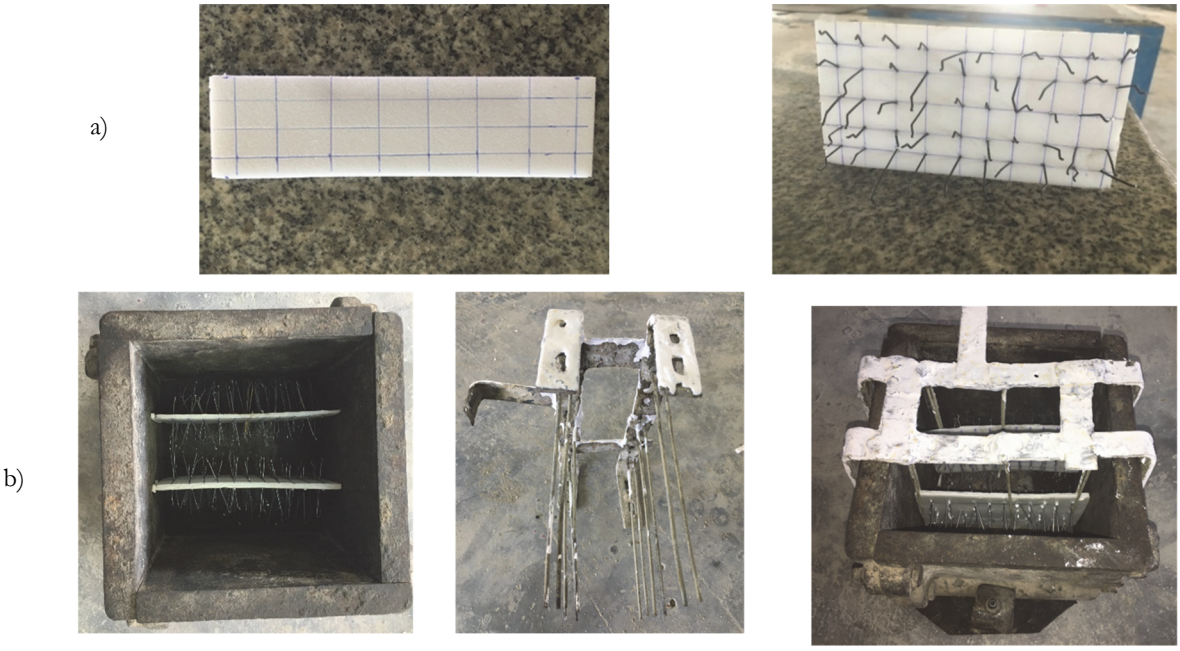

Figure 3: MC preparation sequence. a) Fiber distribution in foam panels; b) Foam panel adjustments in the steel mold.

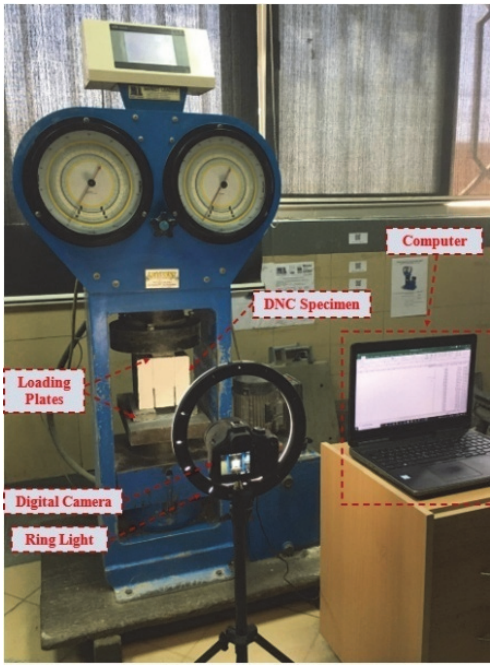

Figure 4: Set up and instrumentation.

Watkins's formula [7] of Mode II fracture toughness (K_{IIC}) measured through DNC specimens was adopted in the present work. He approved that there is a wide range of independence of the geometric size of the specimen, a/w ($0.3 \leq a/w \leq 0.5$), Y(a/w), from compliance, using linear elastic finite element analysis. Therefore, Watkins [7] suggested the following relation for ($0.3 \leq a/w \leq 0.5$):

$$K_{IIc} = \frac{5.11\ P_Q}{2\ B\ w}\sqrt{\pi a} \quad \text{for } (0.3 \le a/w \le 0.5) \tag{1}$$

where K_{IIc} is the mode II fracture toughness in MPa.mm$^{0.5}$, P_Q is the applied load in N, a is the pre-crack length in mm, w is the side length of the cub in mm, and B is the length of the uncracked segment (w-a) in mm, as shown in Fig. 1.

RESULTS AND DISCUSSION

Fracture toughness using DNC specimens

K_{IIC} values for DNC specimens having different values of a/w equal to 0.3, 0.4, and 0.5 are shown in Fig. 5. The figure shows that K_{IIC} increased with the increase of the a/w ratio from 0.3 to 0.5 for all cases of fiber arrangements; the same observation was obtained by Abdallah et al. [17] for mode I fracture toughness K_{IC}. Most recently, Cai et al. [8] found that K_{IIC} did not dramatically change with increasing a/w for DNC specimens with a side length of 100 mm, and they attributed this difference with previous work [25] to the size effect. Therefore, they recommended that further research on size effects is necessary in the future [8]. Furthermore, they [8] concluded that the final failure of the specimens showed a deflection phenomenon due to tensile damage for a/w = 0.3, while 0.4 ≤ a/w ≤ 0.5 was closer to the shear damage.

As illustrated in Fig. 5, the arrangement of the fibers had a significant effect on the measured K_{IIC} for all a/w ratios. MC specimens (with fully distributed fibers throughout the entire specimen and fabricated MC surface) consistently achieved the highest and the realistic K_{IIC}, demonstrating the most effective enhancement of shear resistance. The SCC specimens without fibers show the lowest K_{IIC}. Tab. 6 lists the K_{IIC} values in MPa.mm$^{0.5}$ for DNC specimens having various values of a/w (0.3, 0.4, and 0.5) and different fiber arrangements. A comparison of these values with K_{IIC} of SCC ($K_{IIC\text{-}SCC}$) and K_{IIC} of matrix crack, i.e., real case ($K_{IIC\text{-}MC\text{-}1\%}$), is also presented in Tab. 6. Furthermore, Fig. 6 shows another comparison with respect to a/w. It is clear from Fig. 6 and Tab. 6 that the differences between $K_{IIC\text{-}MC\text{-}1\%}$ and those in the other arrangements are decreased by increasing a/w. However, this trend is not observed if compared with $K_{IIC\text{-}SCC}$, where the highest values of $K_{IIC}/K_{IIC\text{-}SCC}$ were observed at a/w = 0.4 for MC/C and TTC, and a/w = 0.3 for the MC arrangement. On the other hand, the lowest values of $K_{IIC}/K_{IIC\text{-}SCC}$ were observed at a/w = 0.3 for MC/C and TTC, and a/w = 0.5 for the MC arrangement, see Tab. 6.

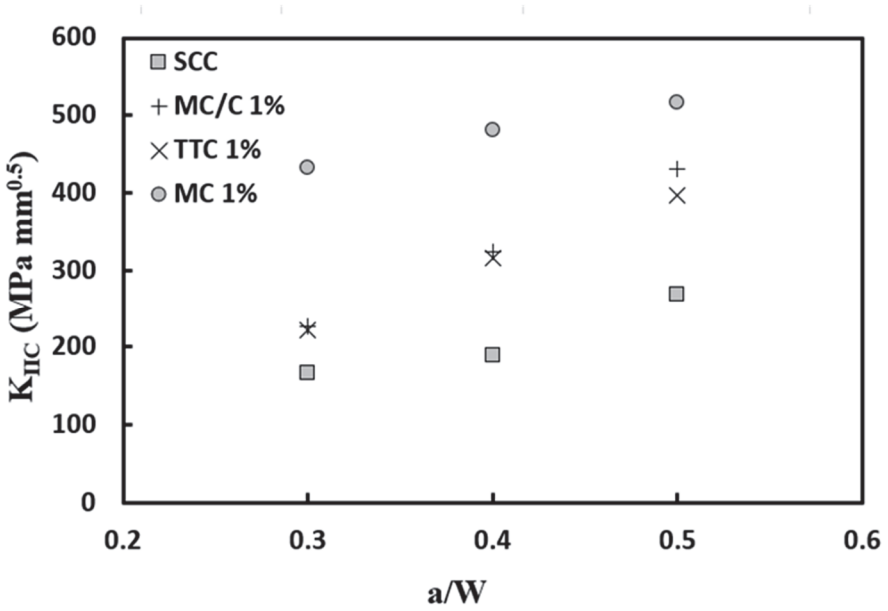

Figure 5: Effect of fiber arrangement on K_{IIC} for different a/w ratios at Vf% = 1%.

The effect of the Vf% increment is also listed in Tab. 6. It is clear that the impact of the a/w ratio has the same trend in the case of MC-1.5%. However, the increase of Vf% from 1% to 1.5% has a marginal effect, which varies between 5%. Overall, the MC/C exhibited better efficiency than TTC, as listed in Tab. 6. This efficiency increased by increasing a/w,

even if these differences were lower by 10%. It can be concluded that the presence of fibers only behind the tip of the crack under pure sliding displacement (pure mode II), to bridge its two surfaces, is more effective than those ahead of its tip. This phenomenon is established in the case of pure opening cracks (pure mode I) [13-18].

Once again, at a/w equals to 0.5, K_{IIC} for SCC-0.5, TTC 1%-0.5, MC/C 1%-0.5, and MC 1%-0.5 were 268, 396, 431, and 517 MPa.mm$^{0.5}$, respectively. As expected, SCC-0.5 had the lowest value of K_{IIC} when the fiber was distributed throughout the entire specimen (TTC 1%-0.5). K_{IIC} increased by about 47.7% compared with SCC-0.5. When the fiber was distributed throughout only the fabricated MC surface (MC/C 1%-0.5), K_{IIC} increased by 8.8% if compared with TTC 1%-0.5; the increase was due to the fiber-bridge effect at the crack, which was more effective than that in the crack path at the shear plane (in case of TTC 1%-0.5). On the other hand, MC 1%-0.5 gives the largest enhancement in K_{IIC} as seen in Fig. 6. In the case of a/w equals 0.3 and 0.4, the same effect of fiber arrangement on the fracture toughness values is observed. K_{IIC} for SCC-0.3, TTC 1%-0.3, MC/C 1%-0.3, and MC 1%-0.3 were 167, 221, 227, and 432 MPa.mm$^{0.5}$, respectively. Adding fiber along the fabricated MC surface (MC/C 1%-0.3) gives 2.7% enhancement above TTC 1%-0.3, this enhancement ratio was less than its counterpart in case of a/w equals to 0.5, this may be due to the larger length of the crack path in the shear plane (in case of TTC 1%-0.3) compared to the crack length, so the fiber-bridge effect was more clear compared to that in the shorter length (crack length in case of MC/C 1%-0.3).

Series name	Vf%	a/w	K_{IIC}	$K_{IIC}/K_{IIC\text{-}SCC}$	$K_{IIC}/K_{IIC\text{-}MC\text{-}1\%}$	
		0.3	167	1	0.39	
SCC	0%	0.4	189	1	0.39	
		0.5	268	1	0.52	$K_{IIC\text{-}MC/C}/K_{IIC\text{-}TTC}$
		0.3	227	1.36	0.53	1.03
MC/C	1.0 %	0.4	323	1.71	0.67	1.02
		0.5	431	1.61	0.83	1.09
		0.3	221	1.32	0.51	
TTC	1.0 %	0.4	316	1.67	0.66	
		0.5	396	1.48	0.77	
						$K_{IIC\text{-}MC\text{-}1\%}/K_{IIC\text{-}TTC}$
		0.3	432	2.59	1	1.95
	1.0 %	0.4	481	2.54	1	1.52
		0.5	517	1.93	1	1.31
MC						$K_{IIC\text{-}MC\text{-}1.5\%}/K_{IIC\text{-}MC\text{-}1\%}$
		0.3	450			1.04
	1.5 %	0.4	505			1.05
		0.5	545			1.05

Table 6: K_{IIC} values in MPa.mm$^{0.5}$ for DNC specimens having different values of a/w (0.3, 0.4, and 0.5) and different fiber arrangements.

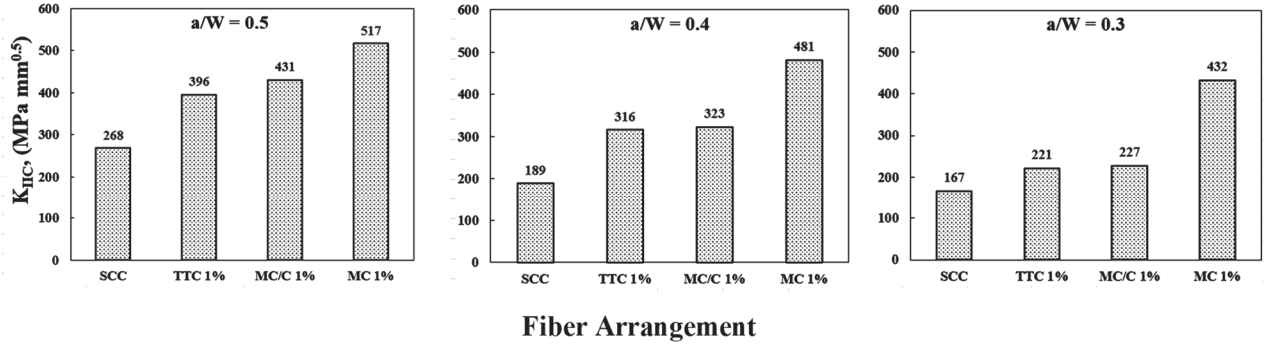

(a) (b) (c)

Figure 6: The effect of the fiber arrangement (Vf%=1%) on K_{IIC} for different values of a/w: (a) a/w = 0.5, (b) a/w = 0.4, and (c) a/w = 0.3.

On the other hand, the same observation in the case of a/w equals 0.4, MC/C 1%-0.4 gives 8.8% enhancement above TTC 1%-0.4, see Fig. 6. The result in the case of a/w equals 0.4, which confirms the conclusion that when the crack length increased compared to the crack path in the shear plane, the effect of the fiber-bridge in MC/C increased the enhancement ratio for K_{IIC}. On the other hand, the largest value of K_{IIC} obtained in MC 1%-0.4 was 481 MPa.mm$^{0.5}$, while the smallest value of K_{IIC} obtained in SCC-0.4 was 189 MPa.mm$^{0.5}$. It can be concluded that both fiber arrangement and the a/w significantly influence K_{IIC}.

Fracture surface shape

The fracture surfaces of the DNC specimens revealed various crack behaviors depending on fiber distribution. In this section, the fracture surface topography will be shown and discussed. The mode of failure of SCC DNC specimens without fiber for different values of a/w is demonstrated in Fig. 7. The crack propagated directly along the predefined shear plane without deviation, confirming pure mode II fracture, and causing a sudden drop after reaching the maximum load due to the absence of the fibers either behind or ahead of the crack tip. For all specimens with a/w ratios equal to 0.3, 0.4, and 0.5, the fracture surfaces appeared smooth and continuous, representing the plain concrete's shear resistance. It is clear that the crack almost grows under pure mode II. It can be concluded that DNC specimens successfully produced a clear shear plane, confirming their effectiveness in isolating pure mode II fracture.

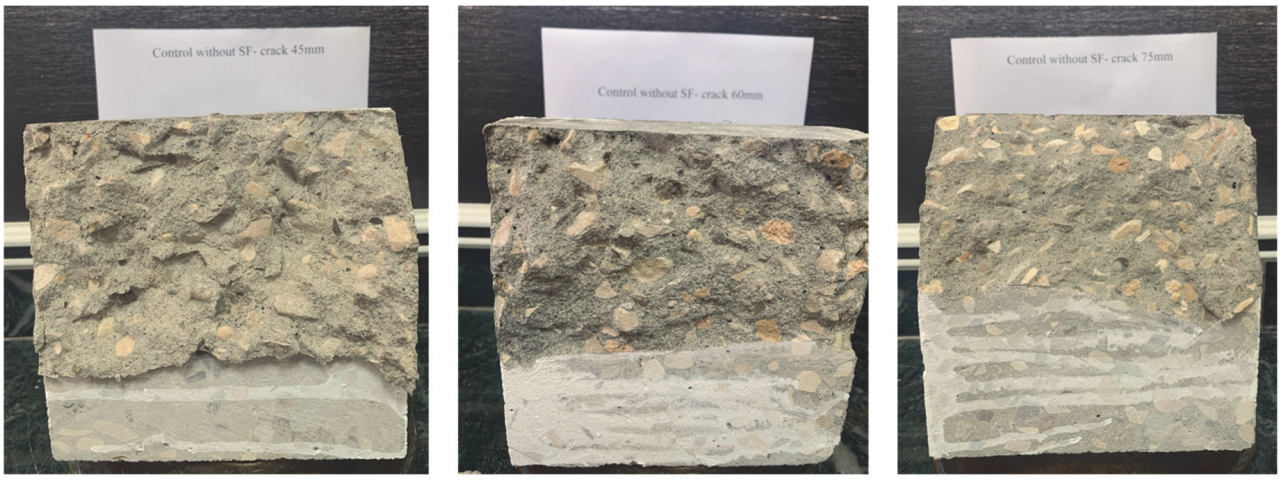

(a) (b) (c)

Figure 7: Fracture surfaces of SCC; (a) (a/w) = 0.3, (b) (a/w) = 0.4, and (c) (a/w) = 0.5.

Fig. 8 illustrates the fracture surfaces of MC/C DNC specimens with fibers localized exclusively along the fabricated MC surface. A high interfacial bond between the mortar and dolomite resulted in transgranular fracture, where the crack propagates directly through the mortar and dolomite. Subsequently, once reaching peak stress, fiber pullout occurred at the specimen's surface. Although fibers are randomly oriented due to different factors such as casting method, dimensions of mold, compaction technique, and concrete mix workability, their closing forces can be analyzed along three perpendicular directions. The most significant direction for studying crack propagation is perpendicular to the crack surface, where fibers provide a bridging effect. Experimental work by Sallam et al [13-19] found the ideal orientation factor to range from 0.3 to 0.48, which supports the widely recommended value of 1/3.

As seen in Fig. 8, the primary mechanism observed is fiber pullout, which occurs as the specimen reaches its maximum stress. The effectiveness of this pullout is pronounced by fiber bridging, where fibers spanning the crack exert closing forces to resist its opening. The efficiency of this bridging is highly dependent on fiber orientation.MC/C configuration allowed direct assessment of how crack-focused fibers influence shear resistance without contributions from fibers outside the crack region.

Fig. 9 illustrates the fracture surfaces of TTC DNC specimens, where the fibers were distributed throughout the entire specimen only. As seen in Fig. 9, the fibers were well-distributed and failed by pullout; the uniform fiber distribution provided consistent bridging and energy dissipation along the crack path, as illustrated by extended fiber pullout. This arrangement did not contribute to effective bridging across the crack plane and offered minimal improvement in shear resistance compared to MC or MC/C configurations.

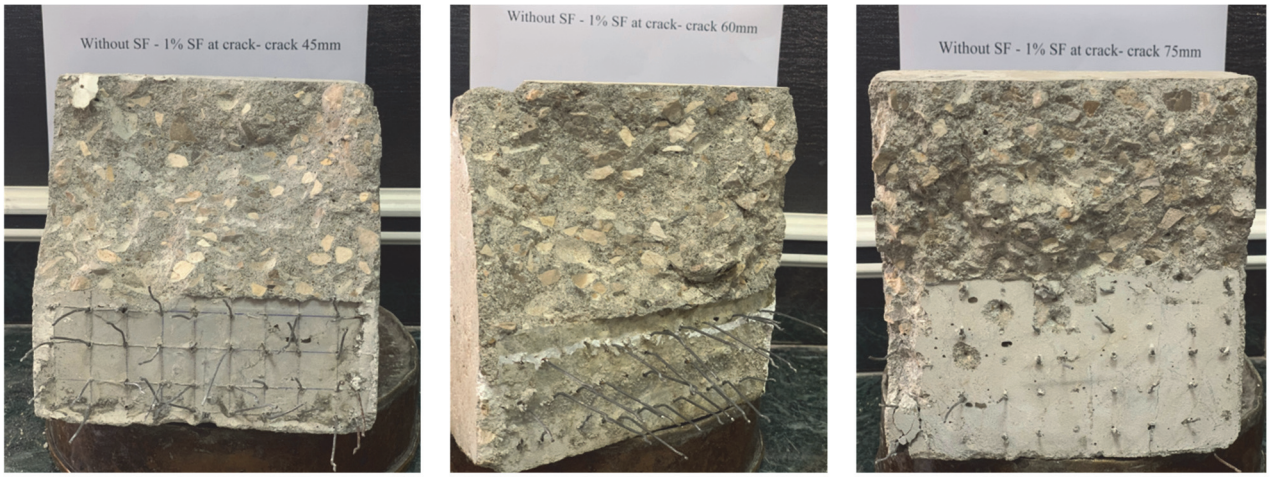

(a) (b) (c)

Figure 8 Fracture surfaces of MC/C; (a) (a/w) = 0.3, (b) (a/w) = 0.4, and (c) (a/w) = 0.5.

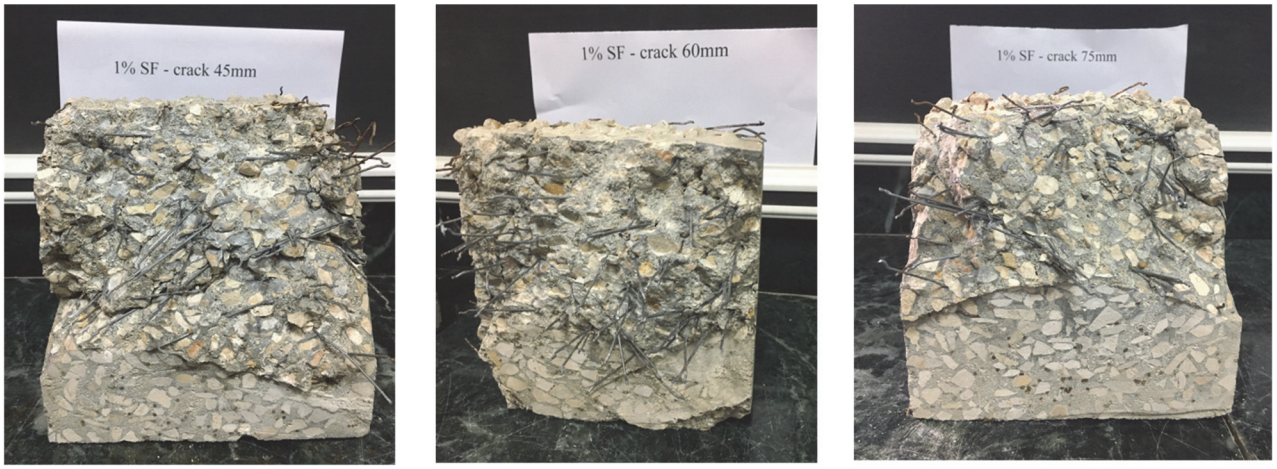

(a) (b) (c)

Figure 9: Fracture surfaces of TTC; (a) a/w = 0.3, (b) a/w = 0.4, and (c) a/w = 0.5.

Fig. 10 illustrates the fracture surfaces of MC DNC specimens with fibers uniformly distributed throughout the entire specimen and a fabricated MC surface with a Vf% equal to 1 and 1.5%. The fracture surfaces show that the hooked-end steel fibers were well-distributed and failed by pullout, as clearly seen in the MC DNC specimens, see Fig. 10.c. The presence of the fibers ahead of the crack tip is crucial for preventing a sudden and brittle failure after the peak load, instead allowing for more ductile mode II crack growth. The crack path, which passed directly through the coarse aggregates, indicates a trans-granular fracture. This was caused by an excellent aggregate-mortar bond, which in turn prevented energy dissipation that would typically occur from crack deviation or aggregate bridging.

Once again, the limited increase in K_{IIC} (approximately 5%) when the Vf% rose from 1% to 1.5% may be due to several factors: First, the efficiency of fiber orientation, which tends to peak and then reach a saturation point, could be a key factor. At 1% Vf, a strong bridging mechanism is already in place. The additional fibers at 1.5% might experience decreased orientation efficiency or begin to cluster, which could limit their effectiveness individually. Secondly, although the fresh properties remained within acceptable ranges, as noted in Tab. 3, the higher fiber content can slightly diminish workability, potentially resulting in a less uniform distribution of fibers. The fracture surfaces support this observation, revealing effective pullout at both fiber percentages, but without a corresponding increase in toughness, suggesting a saturation effect for the pure Mode II sliding resistance in this particular setup.

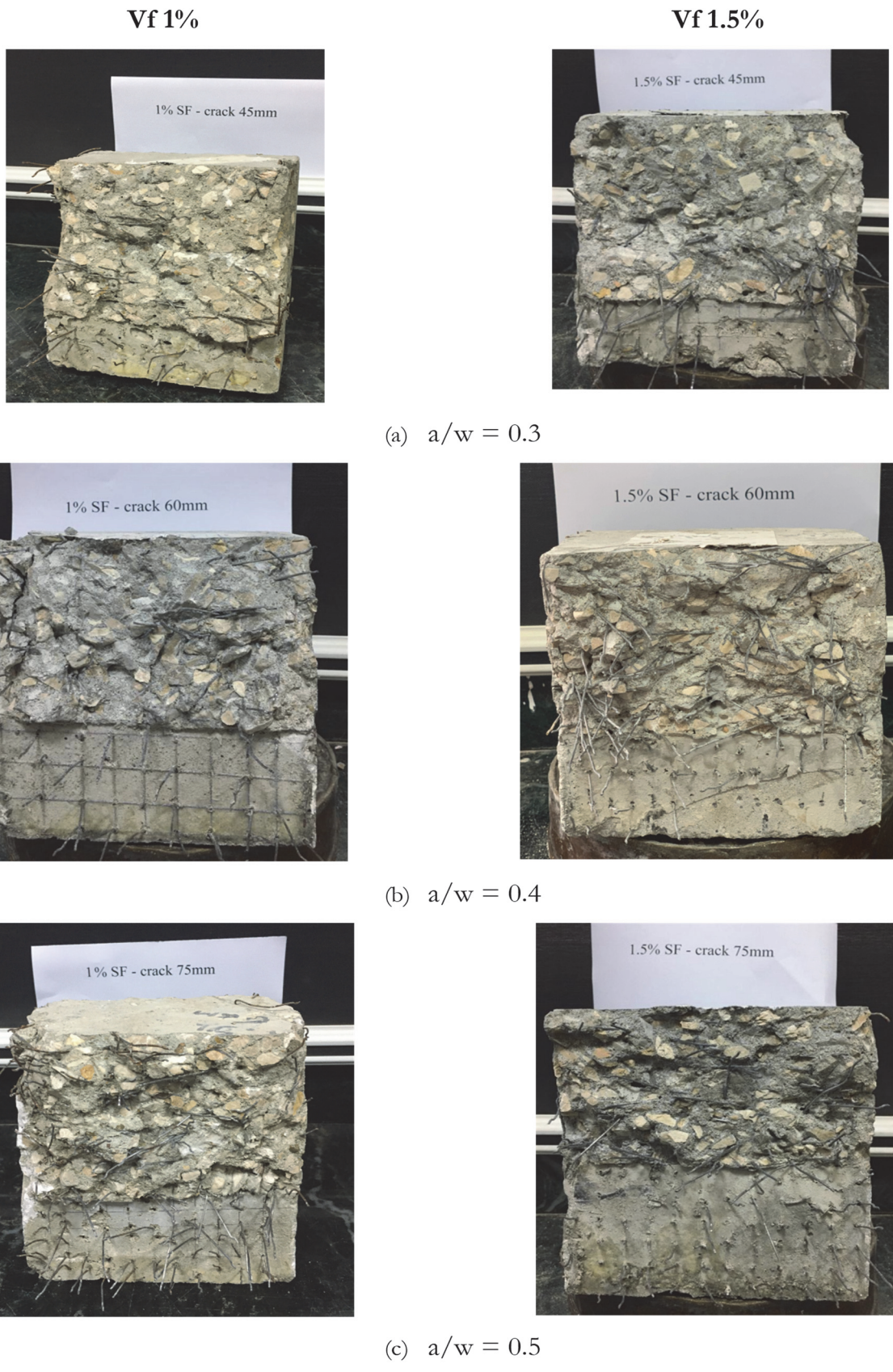

Figure 10: Fracture surfaces of MC for Vf 1% and Vf 1.5%; (a) a/w = 0.3, (b) a/w = 0.4, and (c) a/w = 0.5.

CONCLUSIONS

Matrix cracked DNC specimens were first realized in the present work to measure the actual Mode II fracture toughness of steel fiber reinforced self-compacted concrete. The results of the present experimental work support the following conclusions:

1- TTC DNC specimens are not suitable candidates for measuring accurate values of the K_{IIC} of FRC, where the K_{IIC} values measured through TTC DNC specimens are underestimated compared to the real values of K_{IIC}.

2- MC DNC specimens are suitable candidates for measuring accurate values of the K_{IIC} of FRC.

3- The measured K_{IIC} by MC specimens was higher than that measured by TTC specimens; this difference was more pronounced for a low value of a/w. The ratios of $K_{IIC\text{-}MC\text{-}1\%}$ / $K_{IIC\text{-}TTC}$ are equal to 1.95 and 1.31 for a/w = 0.3 and 0.5, respectively, and are attributed to the presence of fiber bridging behind the crack tip.

4- Comparing $K_{IIC\text{-}MC/C}$ and $K_{IIC\text{-}TTC}$ reveals that the presence of fibers only behind the tip of the crack under pure mode II is more effective than those ahead of its tip; the values of $K_{IIC\text{-}MC/C}$/ $K_{IIC\text{-}TTC}$ ranged between 1.02 and 1.09, establishing that the presence of fibers behind the crack tip is more effective than ahead of the crack tip. This phenomenon is already established in the case of pure mode I.

5- Increasing the fiber volume fraction from 1% to 1.5% has a marginal effect in enhancing $K_{IIC\text{-}MC}$; the values of $K_{IIC\text{-}MC\text{-}1.5\%}$/ $K_{IIC\text{-}MC\text{-}1\%}$ around 1.05.

6- This study showed that the MC approach works well for assessing pure Mode II fracture toughness; however, several limitations need to be noted. The study was performed using one specimen size, 150 mm, under load control. Future research should examine the size effect on the independence of K_{IIC} either under load or displacement control. The behavior under mixed mode (I/II), which is more common in realistic structures, also needs to be studied. Finally, this approach should be applied to different types of FRCs.

REFERENCES

[1] Ghomian, M., Dehestani, M., Garshasbi, S. and Azimi, N. (2025). Optimizing fracture resistance in steel fiber-reinforced self-consolidating concrete: Insights from mode II and mode I fracture energy analysis. Structures, 75, 108707.

[2] El-Nopy, A. M., Noaman, M. T. and Seleem, M. H. (2022). Utilization of Filler Materials in Self-Compacting Concrete as a Partial Cement Replacement. Tehničkivjesnik, 29(3), pp. 867-874.

[3] Ahmad, S. S. E., Gamiaa, G. M. A. and El-Kholy, A. E. M. I. (2024). The effect of beam width and crack-depth ratio on mode I fracture toughness of RCB: an experimental and numerical study. Frattura Ed Integrita Strutturale, 18(67), pp. 24–42. DOI: https://doi.org/10.3221/IGF-ESIS.67.03

[4] Mousa, S., Mutnbak, M., Saba, A. A. M., Abd-Elhady, A. A. and Sallam, H. E. D. M. (2023). Numerical study and experimental validation of the size effect of smooth and mode I cracked semi-circular bend specimens. Scientific Reports, 13(1), 7570.

[5] Mutnbak, M., Abbadi, A., Mousa, S., Abd-Elhady, A. A., Sallam, H. E. D. M. and Reda, R. M. (2025). Effects of specimen geometry and size on mode I and mixed mode fracture behavior of high strength fiber reinforced concrete. Scientific Reports, 15(1), 15286.

[6] Perrella, M., Armentani, E., Lamanna, G. and Berardi, V. P. (2025). Effect of fracture energy estimation on the predictions of mode II behavior of bonded joints using cohesive zone models. Frattura Ed Integrita Strutturale, 19(72), pp. 236–246. DOI: https://doi.org/10.3221/IGF-ESIS.72.17

[7] Watkins, J. (1983). Fracture toughness test for soil-cement samples in mode II. International Journal of Fracture, 23, pp. R135-R138.

[8] Cai, B., Chen, H., Xu, Y., Fan, C. and Tang, Y. (2025). Effect of notch-to-depth ratio on shear fracture properties of plain and fiber-reinforced manufactured sand concrete using double notched cube test. Journal of Building Engineering, 113,114062. DOI: https://doi.org/10.1016/j.jobe.2025.114062

[9] Prokopski, G. (1991). Influence of water-cement ratio on micro-cracking of ordinary concrete. Journal of Materials Science, 26(23), pp. 6352-6356.
[10] Reinhardt, H. W., Ošbolt, J., Shilang, X. and Dinku, A. (1997). Shear of structural concrete members and pure mode II testing. Advanced cement-based materials, 5(3-4), 75-85.
[11] Cao, R. H., Yu, H., Qiu, X., Lin, H. and Cao, M. (2024). Influence of loading rate on the mode II fracture characteristics of SCC samples: Experiments and numerical simulations. Theoretical and Applied Fracture Mechanics, 134, 104729.
[12] Daies, J., Morgan, T.G. and Yim, A.W. (1985). The finite element analysis of a punch-through shear specimen in mode II. International Journal of Fracture, 28, pp. R3-R10.
[13] Ali, A. Y. F., El-Emam, H. M., Seleem, M. H., Sallam, H. E. M. and Moawad, M. (2022). Effect of crack and fiber length on mode I fracture toughness of matrix-cracked FRC beams. Construction and Building Materials, 341, 127924.
[14] Elakhras, A. A., Seleem, M. H. and Sallam, H. E. M. (2021). Intrinsic fracture toughness of fiber reinforced and functionally graded concretes: An innovative approach. Engineering Fracture Mechanics, 258, 108098.
[15] Sallam, H. E. D. M., Elakhras, A. and Seleem, M. (2022). Fracture toughness of matrix cracked FRC and FGC beams using equivalent TPFM. Frattura Ed Integrita Strutturale, 16(60), pp. 73-88.
[16] Elakhras, A. A., Seleem, M. H. and Sallam, H. E. M. (2022). Real fracture toughness of FRC and FGC: size and boundary effects," Archives of Civil and Mechanical Engineering, 22(2).
DOI: https://doi.org/10.1007/s43452-022-00424-6.
[17] Abdallah, M. A., Elakhras, A. A., Reda, R. M., Sallam, H. E. D. M. and Moawad, M. (2023). Applicability of CMOD to obtain the actual fracture toughness of rightly-cracked fibrous concrete beams. Buildings, 13(8), 2010.
[18] El-Sagheer, I., Abd-Elhady, A. A., Sallam, H. E. D. M. and Naga, S. A. (2021). An assessment of ASTM E1922 for measuring the translaminar fracture toughness of laminated polymer matrix composite materials. Polymers, 13(18), 3129.
[19] Hussien, M. A., Moawad, M., Seleem, M. H., Sallam, H. E. M. and El-Emam, H. M. (2022). Mixed-mode fracture toughness of high strength FRC: a realistic experimental approach. Archives of Civil and Mechanical Engineering, 22(4), 168.
[20] EFNARC, F. (2002). Specification and guidelines for self-compacting concrete. European Federation of Specialist Construction Chemicals and Concrete Systems.
[21] BS EN 12390–12393; Testing Hardened Concrete-Compressive Strength of Test Specimens, Part 3. British Standards: London, UK, (2009).
[22] BS EN 12390–12396; Testing Hardened Concrete. Tensile Splitting Strength of Test Specimens, Part 6. British Standards: London, UK, (2009).
[23] Barragan, B., Gettu, R., Agullo, L. and Zerbino, R. (2006). Shear failure of steel fiber-reinforced concrete based on push-off tests. ACI materials journal, 103(4), 251.
[24] BS 1881; Specification for compression testing machines for concrete, Part 115. British Standards: London, UK, (1986).
[25] Abou El-Mal, H. S. S., Sherbini, A. S. and Sallam, H. E. M. (2015). Mode II fracture toughness of hybrid FRCs. International Journal of Concrete Structures and Materials, 9(4), 4pp. 75-486.